Design and characterization of a prototype proton response matrix for the XMM-Newton mission

V. Fioretti, T. Mineo, R. Amato, S. Lotti, C. Macculi, et al.

V. Fioretti, T. Mineo, R. Amato, S. Lotti, C. Macculi, S. Molendi, F. Gastaldello, G. Lanzuisi, M. Cappi, M. Dadina, S. Ettori, "Design and characterization of a prototype proton response matrix for the XMM-Newton mission," Proc. SPIE 11822, Optics for EUV, X-Ray, and Gamma-Ray Astronomy X, 118221F (23 August 2021); doi: 10.1117/12.2594120

SPIE.

Event: SPIE Optical Engineering + Applications, 2021, San Diego, California, United States

Design and characterization of a prototype proton response matrix for the XMM-Newton mission

V. Fioretti[a], T. Mineo[b], R. Amato[b], S. Lotti[c], C. Macculi[c], S. Molendi[d], F. Gastaldello[d], G. Lanzuisi[a], M. Cappi[a], M. Dadina[a], and S. Ettori[a]

[a]INAF OAS Bologna, Via P. Gobetti 93/3, I-40129 Bologna, Italy
[b]INAF IASF Palermo, Via U. La Malfa 153, I-90146 Palermo, Italy
[c]INAF IAPS, Via del Fosso del Cavaliere, 100, I-00133 Roma, Italy
[d]INAF IASF Milano, Via A. Corti 12, I-20133 Milano

ABSTRACT

Low energy (< 200 keV) protons entering the field of view of the XMM-Newton telescope and scattering with the mirror surface are observed in the form of a sudden increase in the background level. Such flaring events, affecting about 30-40% of XMM-Newton observing time, can hardly be disentangled from true X-ray events and cannot be rejected on board. A response matrix for protons would allow a better understanding of the proton radiation environment, with the aim of modeling the in-flight non X-ray background of current (e.g. XMM-Newton, eROSITA) and future (e.g. ATHENA) X-ray focusing telescopes. Thanks to the latest validation studies on the physics models describing the reflection process of protons at grazing angles, we propose to build a prototype XMM-Newton EPIC proton response matrix describing the effective area and energy redistribution of protons entering the mirror aperture. The simulation pipeline comprises two independent simulation frameworks for the X-ray optics reflectivity, based on ray-tracing and Geant4, and a Geant4 simulation for the proton transmission efficiency caused by the combination of optical filters, on-chip electrodes and the detection depletion regions, requiring a detailed mass model of the MOS focal plane assembly. We present here the pipeline design, the characterization and verification of the proton transmission efficiency, and the algorithms for the effective area and energy redistribution computation. After the verification and validation activity, an opportune data formatting of the tool and its interface with widely-used analysis software (e.g. XSPEC) will allow the distribution of the proton response matrix to the scientific community.

Keywords: XMM-Newton, soft protons, background

1. INTRODUCTION

The ESA XMM-Newton X-ray mission was launched in December 1999 and in more than 20 years, and counting, of operations has provided a unique observation window to the X-ray Universe at energies below 10 – 15 keV. Orbiting in high eccentricity elliptical orbit, with an apogee $> 10^5$ km, XMM-Newton carries three Wolter type-I mirrors to focus X-rays by means of grazing angle reflection with European Photon Imaging Cameras (EPIC) placed at each focal plane. Together with observations of Active Galactic Nuclei, Supernova remnants and clusters of galaxies, XMM-Newton also led to the discovery that low energy protons (< 200 keV) entering the field of view can generate photon-like deposits that can hardly be disentangled from the X-ray events and consequently cannot be rejected on board.

The scattering of low energy protons at the surface of X-ray mirrors was discovered after the degradation of the front-illuminated Chandra ACIS CCDs[1] a few months before XMM-Newton launch. The telescope instruments are protected from damage by closing the filter wheel when crossing the radiation belt but sudden increases in the background rate are still observed along the entire orbit.[2]

These so-called soft proton flaring events can prevail over the quiescent background level up to 1000%, with the loss of up to 40% of observing time.[3] While shielded by the Earth's magnetic field below the radiation belts,

Contact author: V. Fioretti
E-mail: valentina.fioretti@inaf.it

Optics for EUV, X-Ray, and Gamma-Ray Astronomy X, edited by Stephen L. O'Dell, Jessica A. Gaskin, Giovanni Pareschi, Proc. of SPIE Vol. 11822, 118221F · © 2021 SPIE · CCC code: 0277-786X/21/$21 · doi: 10.1117/12.2594120

low energy protons populate both the interplanetary space and the outer magnetosphere, including the Earth's magnetotail,[4] in the form of a steady flux characterized by both short and long term variability induced by transient shock waves (e.g. coronal mass ejections) and the solar activity cycle. All future high throughput X-ray telescopes operating outside the radiation belts (e.g. the ESA Athena X-ray observatory planned for launch on 2031) are potentially affected by contamination induced by soft protons, and their effects must be then foreseen and limited since the design phase.

The simulation of the soft proton induced background requires a dedicated modeling of the radiation environment encountered by the spacecraft, the proton transmission efficiency through the mirror module, filters and its final interaction with the detection system. The validation of the simulation chain can only be obtained by comparison of the predicted background flux with in-flight data. In this context, XMM-Newton provided an unprecedented archive of soft proton flare spectra and represents a unique laboratory for the characterization of the detection response towards low energy protons entering the field of view. At the same time, once the response is validated against in-flight data, we can derive from XMM-Newton detected flares the proton flux encountered along the orbit, improving our knowledge of the near-Earth radiation environment.

We present here the design and development plan of a proton response matrix for the XMM-Newton telescope (Sect. 2), composed by a Redistribution Matrix File (RMF) mapping the proton energy space (from tens to hundreds of keV) into detector pulse height and an Auxiliary Response File (ARF) collecting the grasp of the optics, the filter transmission efficiency and the detector quantum efficiency. The proton interaction with the X-ray optics is simulated with two independent frameworks (Sect. 3) based on ray-tracing and Geant4, to verify the mirror geometry and physics implementation. The focal plane assembly (Sect. 4) is simulated in Geant4 and verified against on-ground calibration measurements and analytical computations. Preliminary results obtained with a prototype proton response matrix using the ray-tracing elastic Remizovich as scattering model, the EPIC MOS detection system and the medium optical filter configuration are summarized in Sect. 5.

2. PROTON RESPONSE MATRIX DESIGN

A preliminary simulation of the soft proton induced background, using a simplified model of the X-ray mirror and the EPIC pn detector (Sect. 4.2) was published in this work,[2] but the validation against real data was not possible because of (i) the lack of in-flight data averaged along the spacecraft orbit, (ii) the lack of a precise estimate of the proton environment and (iii) the use of approximated scattering physics models. In recent years, the EXTraS (Exploring the X-ray Transient and variable Sky) project,[5] funded by the FP7 European program, provided an unbiased database of XMM-Newton EPIC blank sky observations for the characterization of the focused charged particle background collected in 13 years of data. In parallel, measurements of proton scattering at grazing angles ($< 1-2$ degrees) on the surface of samples of the Athena Silicon Pore Optics* and eROSITA X-ray mirror,[6] and the comparison with simulations, have defined with sufficient accuracy the driving physics model for the reflection of protons at grazing incident angles. The need for accurate estimates of the particle background on board the Athena mission has fostered an in depth study of the soft proton environment in L1 and L2 with the definition of fluxes and spectral distribution for different solar conditions.[7] With this improved knowledge of the environment, the proton physics interaction and the in-flight observations, we can now build a verified and optimized simulation of the X-ray mirror and focal plane assemblies.

A first version of the XMM-Newton proton response matrix[8] tested the feasibility of the method in producing a simulation tool with a wide range of applicability. By simulating mono-energetic proton beams at the mirror entrance, we can in fact encode the proton transmission efficiency and energy losses into the same instrument response used to deconvolve the detected X-ray spectra into the source model. The response matrix is formatted according to the NASA OGIP (Office of Guest Investigators Program) calibration database (caldb) format, and it consists into an RMF and ARF file in FITS (Flexible Image Transport System) format. Any X-ray data analysis tool available to the X-ray astronomy community (e.g. XSPEC,[9] SPEX[10]) can be used to simulate the soft proton induced background spectra, for any given condition of the orbit proton environment without the need to run again the simulation pipeline. Alternatively, the possibility to convert the observed spectra and rates to the ones hitting the telescope pupil would improve our knowledge of the near-Earth radiation environment.

*Provided by the ESA funded EXACRAD (Experimental Evaluation of ATHENA Charged Particle Background from Secondary Radiation and Scattering in Optics) project (ESA contract n° 4000121062/17/NL/LF).

The simulation pipeline logical schema is shown in Fig. 1 (left panel). The mirror simulation is performed with two independent simulation frameworks using ray-tracing and the Geant4 toolkit,[11,12] in order to verify the geometry and physics models and estimate potential systematic effects in their implementation. The output of both simulators is processed and an event list, storing energy and angular distribution of the protons at a given distance from the focal plane, is extracted and given as input to a Geant4 simulation of the focal plane assembly (FPA), including baffles, optical filters and the detectors. From the FPA simulation, we reconstruct the counts on the EPIC CCDs, applying a pattern flag, according to the instrument read-out configuration, and a *baffle* flag for the protons that interact with the radiation shielding before reaching the detector. The product of this processing stage is a data level 1 FITS file listing the count energy, position, pattern and baffle flags, one for each Geant4 simulation run of each input energy. In the data level 2 we compute for each input energy the energy probability distribution in the instrument channels, normalized to 1, and the grasp. For X-ray photons, that are mono-directional, the response ARF file is the product of the effective area of the mirror, i.e. geometric area multiplied by the reflection efficiency, the filter transmission efficiency and the detector quantum efficiency. For the soft proton environment, we assume an isotropic distribution at the mirror entrance and the input aperture angle used in the simulation must be taken into account when computing the total transmission efficiency. The simulated grasp is the product of the system efficiency multiplied by the proton aperture solid angle at the mirror entrance, in units of cm^2 sr. The data level 2 files are then unified and formatted into the OGIP RMF and ARF response files. A different proton response will be produced for each combination of mirror simulator, optical filter type, and focal plane instrument.

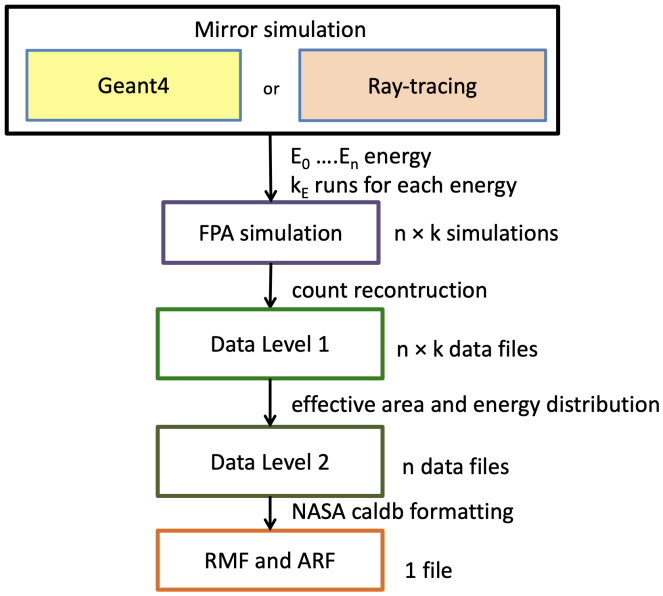

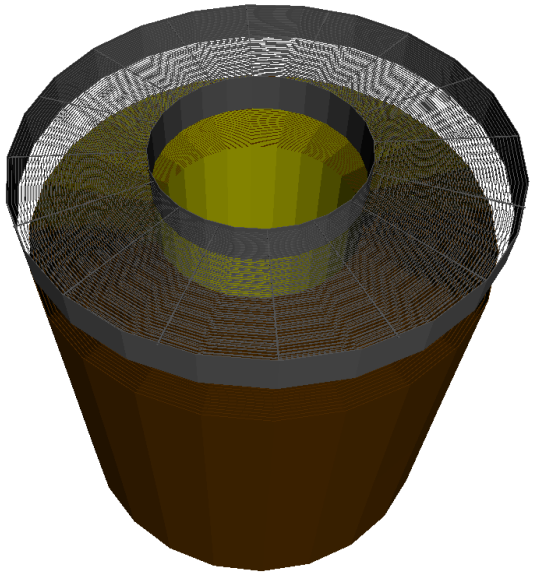

Figure 1. *Left panel*: Simulation and post-processing software pipeline logical schema. *Right panel*: Geant4 mass model of the XMM-Newton mirror module including the X-ray baffle placed at the telescope pupil.

3. X-RAY MIRROR SIMULATION

Each X-ray mirror module consists of 58 Wolter type-I coaxial and cofocal Gold-coated Nichel shells[13] composed by a paraboloid and hyperboloid section, with a thickness ranging from 0.47 mm at the inner shell, with a diameter of $\sim$ 30 cm, to 1.07 mm at the outer 70 cm diameter. The coating thickness is 0.2 μm and the focal length is 7.5 m. An X-ray baffle is placed at the entrance for stray-light suppression in the field of view of the instruments. Its inclusion is mandatory in the mirror simulation because it also reduces the incoming proton flux. The baffle is made of Invar, a Nickel-Iron alloy commonly used for space applications because of its low coefficient of thermal expansion, and it consists of two planes of 59 circular strips and 16 radial spokes at about 10 cm from the mirror entrance.

The Geant4 mass model of one XMM-Newton mirror module is shown in Fig. 1 (right panel), with in grey the X-ray baffle, dark red the Nickel shells and yellow the Gold coating visible in the inner regions. The ability to reproduce the proton scattering interaction with the mirror surface is a key ingredient in the simulation of soft proton induced background. Geant4 simulations were compared to experimental measurements of proton scattering first in this work,[14] using eROSITA data collected from literature,[15] and lately within the ESA funded EXACRAD project that provided original experimental data using samples of the Athena X-ray mirror. The new detailed validation of Geant4 physics scattering models, the Geant4 reference Single Scattering physics list and the AREMBES Space Physics List (SPL), together with a comprehensive estimate of the systematic uncertainties introduced by the experiments, proved[16] the Coulomb scattering to reproduce experimental observations with sufficient accuracy. Fig. 2 shows the simulated and measured[6] proton scattering efficiency as a function of the scattering angle, using a sample of eROSITA for an incident angle of 0.5° and an input energy of 300 keV. Both the Single Scattering, as provided by the Geant4 10.4 reference physics list, and the SPL, with a 1 nm production cut and a modified step limiter of 0.1 nm, are able to reproduce the measurement within 1σ. Since the eROSITA

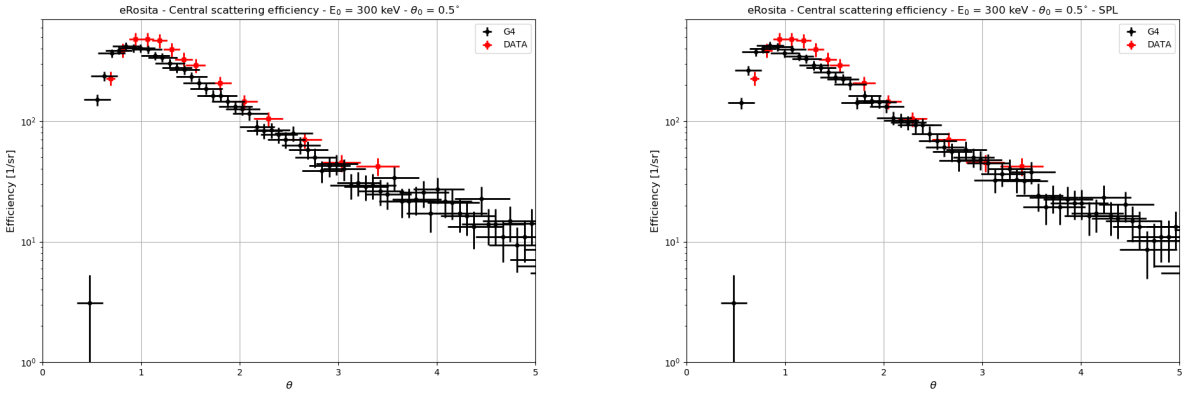

Figure 2. Comparison between simulated and measured proton scattering efficiency at a sample of eROSITA mirror shells for an incident angle of 0.5° and an input energy of 300 keV. The physics scattering model is provided by the Geant4 reference Single Scattering physics, left panel, and the ESA AREMBES SPL (right panel).

target is composed by a Nickel substrate of 270 μm coated by 50 nm of Gold, hence very similar to the design of the XMM-Newton X-ray telescope, we can extend the same Geant4 physics modeling to the proton response matrix simulation.

The ray-tracing code is a stand-alone software that includes the XMM-Newton optics geometry, the optics baffle and the forward proton shield in front of the detectors. It is able to handle either photon and protons. It follows the particle from the pupil through its interactions with the mirror shells down to the focal plane. At each interaction, it uses a Monte Carlo method to assign the particle angular and energy distribution according to a defined probability model. The photon reflectivity is modeled according to tabulated values[17,18] and the mirror micro-roughness is taken into account modifying the output specular direction with a Gaussian. The optics geometry has been verified comparing the ray-tracing values of the X-ray on-axis effective area and vignetting at 1.5 keV and 6.4 keV with the nominal ones[†]. Discrepancies between the two sets of curves are always lower than 5%. Two proton reflection models are implemented in the XMM-Newton mirror simulation code:

- the Remizovich model in elastic approximation that assumes a reflection efficiency of 100% and no energy degradation. The output angular distribution is drawn from the Remizovich formulas.[19]
- a modified version of the Remizovich model in non-elastic approximation, based on laboratory measurements on eROSITA mirror samples that include the energy lost in the interactions.[20] In this model the

[†]Effective area curve from http://xmm.esac.esa.int/external/xmm_user_support/documentation/technical/Mirrors/index.shtml Vignetting curves from https://xmm-tools.cosmos.esa.int/external/xmm_user_support/documentation/uhb/effareaoffaxis.html

dimensionless parameter σ of the Remizovich solution, that summarizes the physics of the proton interaction with matter, is directly determined by fitting experimental data. The parameter σ is found to be independent from the energy of the incident protons, with a dependence on the incidence angle θ_0, given by:

$$\sigma = 88 \times \theta_0^{-0.9} . \quad (1)$$

The current prototype response matrix uses the elastic Remizovich model obtained with the ray-tracing code, in order to better characterize the proton energy losses in the FPA.

4. FOCAL PLANE ASSEMBLY

The spacecraft carries three X-ray EPIC cameras, each at the focal plane of the three mirror modules. Two of the cameras are MOS (Metal Oxide Semi-conductor) CCD arrays,[21] where the presence of Reflection Grating Spectrometers (RGS) behind the X-ray telescopes shadows about 50% of the incoming proton flux. The third EPIC camera uses pn CCDs[22] and no RGS is present. The FPA surrounding the three cameras is the same, including a filter wheel, door, and radiation shielding baffles, the latter composed by a Titanium forward proton shield, 100 mm long, and an Aluminum alloy baffle about 60 cm long placed at the top of the filter wheel (Fig. 3, left panel). While the presence of the radiation shielding is fundamental in reducing the non-focused particle induced background (e.g., induced by galactic cosmic rays), in case of protons entering the field of view the secondary scattering at the baffle inner surface can potentially increase the background rate (see Sect. 5). The

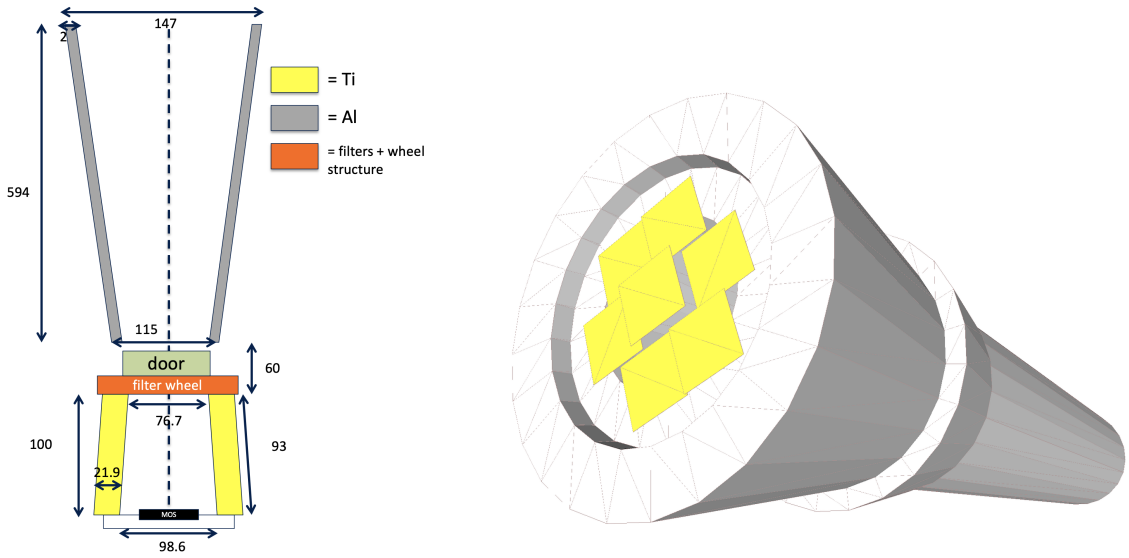

Figure 3. Schematic view of the XMM-Newton focal plane assembly geometry (left panel) and the respective bottom view of the Geant4 mass model, with highlighted in yellow the MOS CCDs.

filter wheel is equipped with three different optical blocking filters,[22] to reduce contamination from IR, visible and UV light collected in the field of view. With a diameter of 76 mm and placed at 10 cm from the focal plane, the observer can select among two thin filters, made of 0.16 μm of Polymide (Pl) and 0.04 μm of Aluminum (Al), 1 medium filter, made of 0.16 μm of Polymide and 0.08 μm of Aluminum, and a thick filter, with 0.33 μm of Polypropylene (PP), 0.11 μm of Aluminum and 0.045 μm of Tin (Table 1).

4.1 The MOS camera

The MOS camera is composed by 7 front-illuminated CCDs operating from 0.5 to 12 keV (Fig. 3, right panel). Each CCD is divided into 600×600 pixels, each with an area of 40×40 μm^2. The central CCD is at the focal point on the optical axis of the telescope, while the others are at a distance of 4.5 mm towards the mirror, to approximately reproduce the focal plane curvature. The MOS conventional 3-phase front-illumination device is

XMM-Newton optical filters

Filter	Layer 1	Layer 2	Layer 3
thin	Al (0.04 μm)	Pl (0.16 μm)	
medium	Al (0.08 μm)	Pl (0.16 μm)	
thick	Tin (0.045 μm)	Al (0.11 μm)	PP (0.33 μm)

Table 1. The composition and thickness of the optical blocking filters. The layer numbering starts at the mirror side.

characterized by an open electrode structure,[23] where one of the electrodes was partially etched, i.e. holes were cut through it, to increase the X-ray detection efficiency at low energies. The resulting device structure[24,25] is divided into a 60% portion covered by the standard *closed* electrode structure, composed by a layer of Si (0.3 μm thick) and SiO_2 (0.75 μm thick), and a 40% area of *open* electrode with only 0.085 μm of SiO_2. The depletion region, made of Silicon, is 37 μm thick. Fig. 4 (left panel) shows a not in scale schema of the pixel geometry implemented in Geant4. The X-ray detection efficiency generated by the MOS CCD pixels was measured on-

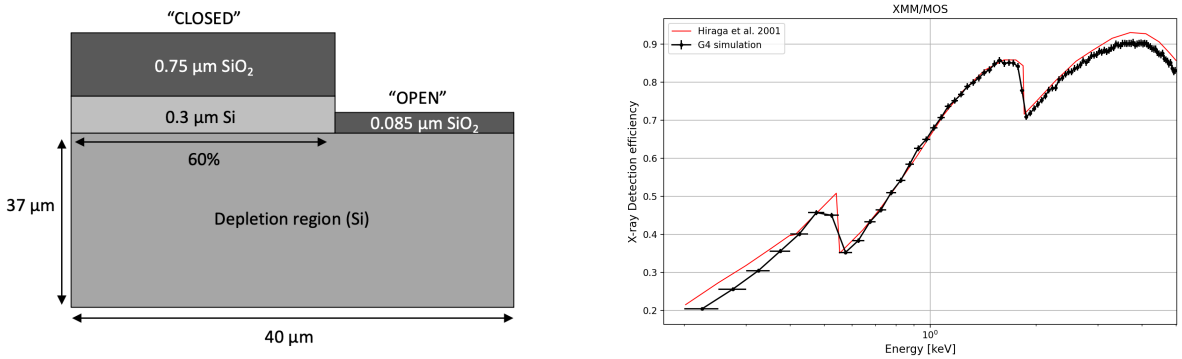

Figure 4. *Left panel:* Schematic side view, not in scale, of the MOS pixel geometry implemented in the simulation, with the open and closed electrode structure on top of the depletion region covering 60% and 40% of the pixel area respectively. *Right panel*: Comparison of the measured (red line) and simulated (black line) MOS X-ray detection efficiency.

ground by sampling different positions of the array.[24] The resulting mean pixel X-ray response is compared in Fig. 4 (right panel) to the Geant4 simulation of the MOS quantum efficiency obtained by illuminating the array with a uniform photon beam from 0.2 to 5 keV. Given the simplified electrode geometry implemented in Geant4, the consistency of the two curves verifies the correct simulation of the MOS camera, a key factor in correctly estimating the proton energy losses.

4.2 The pn camera

The pn camera is instead back-illuminated, composed by four quadrants each having three CCDs with 200×64 pixels, with a pixel size of 150×150 μm and a total imaging area of 6×6 cm. The fully depleted Silicon thickness is 300 μm. Being back-illuminated, no read-out devices are present in front of the pn camera, simplifying its Geant4 implementation.

5. PRELIMINARY RESULTS

The presence of the metalwork in front of the MOS, shadowing a region of the camera, provides during data taking simultaneous out and in field of view background observations. During soft proton flares, the contribution of the unfocused Non X-ray Background can be subtracted from the total count rate, providing easy access to unbiased X-ray detections of the soft proton component. For this reason, for the release of the first prototype of the XMM-Newton proton response matrix, we selected the MOS camera (medium filter) to help the validation process against in-flight data. Mono-energetic protons are simulated in the 8 – 200 keV energy range. The

reconstruction of the energy distribution follows the X-ray instrument response data format, with a total of 800 channels, an energy width of 15 eV and energy boundaries of 0 – 12 keV.

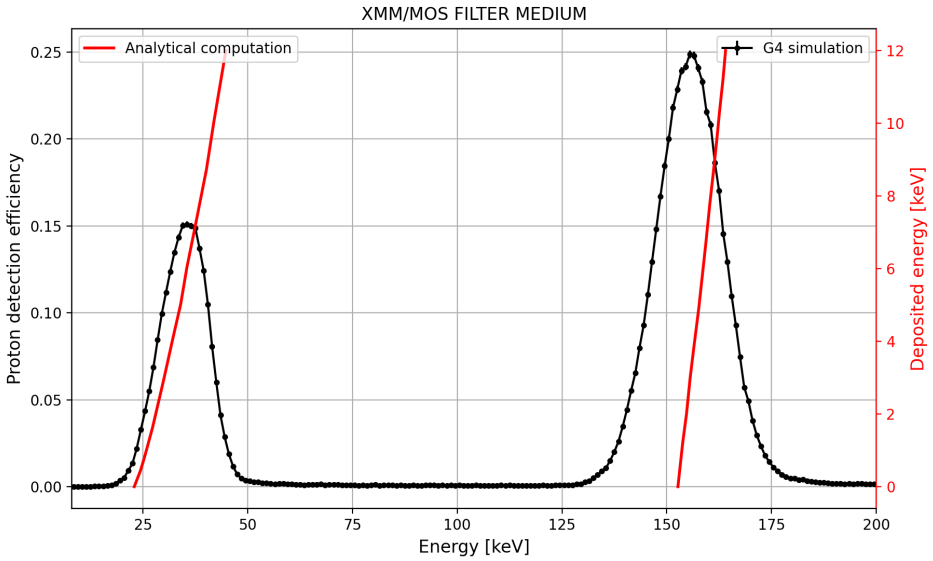

Figure 5. Simulated, in black, proton transmission efficiency in the 8 – 200 keV energy range for the MOS and medium filter. The analytical computation based on tabulated NIST proton stopping power predicts the proton energy range for which the MOS is likely to register a count, with an energy labelled by the red y-axis.

5.1 Transmission efficiency

The total transmission efficiency, using parallel mono-energetic proton beams, allows to define the required input proton for each end-to-end simulation (mirror and FPA) to reach an equal statistics throughout the energy range. Protons are randomly generated within a circle with a diameter of 76 mm (equal to the filters), centered on the optical axis of the telescope and perpendicular to it. Proton energies are randomly generated in the range 8–200 keV, and then selected in the analysis in bins of 1 keV to evaluate the transmission efficiency. The latter is defined as the number of protons that deposit energy within the MOS energy range (0.03 - 12 keV) over the total number of simulated protons within the bin. The result is shown in Fig. 5, where two peaks in the transmission efficiency appear, one centered at $\sim$ 35 keV if protons cross the open electrode, and one centered at $\sim$ 160 keV if they encounter instead the thicker closed electrode. For the analytical computation, proton stopping powers reported by NIST [‡] were used for all of the materials involved. The stopping power curves were interpolated using Mathematica[§], and the energy loss after each layer of the filters and the electrodes was calculated as a function of their thickness. As a result, we obtained the energy of the proton when impacting on the sensitive layer of the MOS detector, as a function of the incident energy and the thickness of each layer crossed by the particle, that were left as free controllable parameters in the computation to allow probing different configurations. The analytical computation defines an energy range where protons are able, according to the tabulated stopping power, to reach the MOS pixels without losing all their energy. Not only the two peaks predicted by the Geant4 simulations are confirmed by the tabulated stopping power, but the energy ranges are also consistent if we consider the uncertainties introduced by the angular spread and the complex geometry of the pixels.
The proton energy and angular distribution at the exit of each layer was analyzed for a set of energies to verify the analysis pipeline processing the FPA simulation. Fig. 6 shows the result for a 35 keV input proton beam, where the transmission efficiency low energy peak is centered. About 20 keV are lost in the medium filter, and

[‡] https://physics.nist.gov/PhysRefData/Star/Text/PSTAR.html
[§] Wolfram Research, Inc., Mathematica, Version 9.0, Champaign, IL (2012)

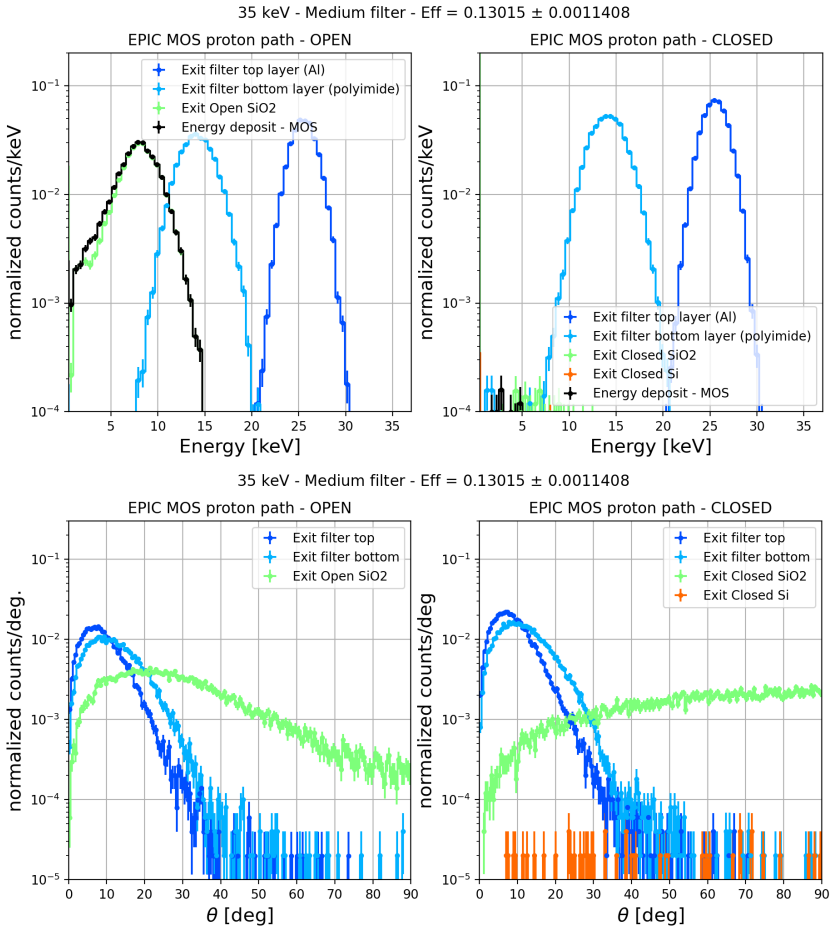

Figure 6. Energy and angular distribution of the protons, for an input energy of 35 keV, exiting each layer of the medium filter and electrode structure, open in the left panel and closed in the right panel.

while the closed electrode absorbs the remaining energy, if protons reach the open structure their final energy falls in the 5–10 keV band. The proton direction spread, defined as the angle from the telescope axis, increases linearly while crossing the passive layers, and the medium filter alone introduces a $5° - 10°$ medium shift. This angular spread impacts the number of protons that are able to reach the detector, and the height of the filter from the focal plane is a parameter that can modify the soft proton induced background. The front-illuminated device increases drastically the spread, and the protons lose memory of their incident direction.

5.2 Spectral and spatial distribution at the detector

The impact of the proton shield in scattering soft protons coming from the field of view is tested by extracting the output of the mirror simulation at two heights: 754 mm, the focal plane baffle entrance, and 111 mm, at the optical filter. Using the baffle flag of the data level 1 (Sect. 2), we can estimate the fraction of protons that scatter with the focal plane baffle before generating the background event. The result is shown in Fig. 7. The fraction of proton that scatter with the radiation shielding increases from $\sim 2\%$ for an height of 111 mm (left panel) to $\sim 20\%$ for the 754 mm case (right panel). Protons scattering with the baffle surface lose energy and increase the low energy tail of the spectrum, and this effect is clearly visible in the plot. While for a single input energy the contamination induced by secondary scattering is negligible, its effect integrated from 8 to 200 keV can soften the background spectral distribution and will be included in the official response matrix release. The pattern analysis shows that 99.9% of the simulated counts has a pattern of 0, i.e. only one pixel triggered for each event, as in the in-flight Non X-ray Background.[26] The counts map and their radial distribution on the CCDs is shown in Fig. 8, with the metalwork placed in front of the camera shadowing the focal plane region at a diameter

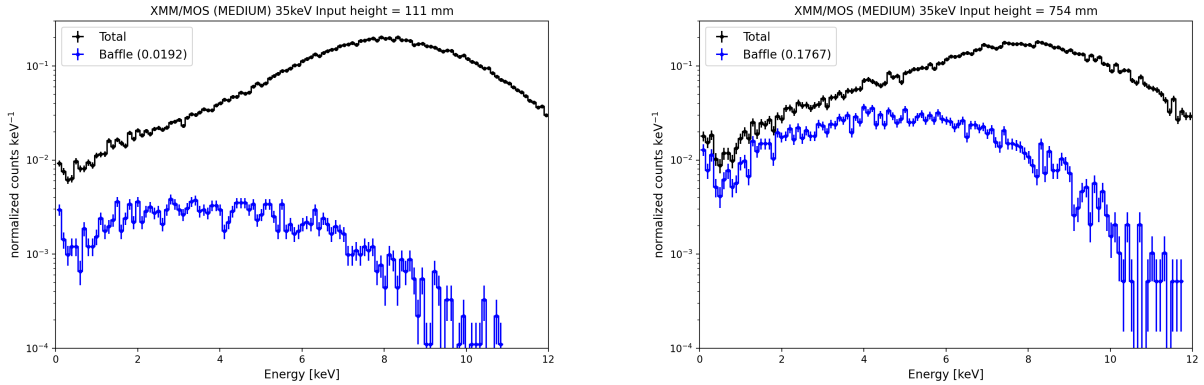

Figure 7. Soft proton induced X-ray spectra, for an incident energy of 35 keV, obtained extracting the mirror simulation proton list at an height of 111 mm (at the optical filter, left panel) and 754 mm (the baffle entrance, right panel). Protons interacting with the baffle surface before generating a count on the MOS are highlighted in blue, and their fraction with respect to the total is reported in the legend.

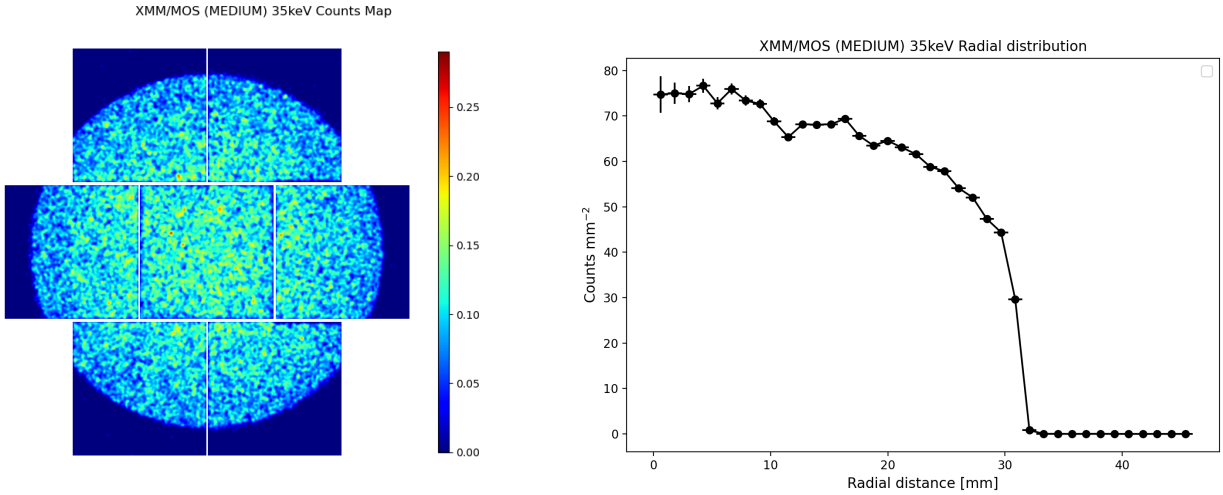

Figure 8. Counts map detected at the MOS camera for an input proton energy of 35 keV (left panel) and related radial distribution (right panel), with the vignetting effect clearly visible.

larger than 62 mm. The radial distribution is obtained by dividing the MOS in annular regions from the center and computing the surface density, in counts mm^{-2}. A vignetted distribution, i.e. the intensity reduction from the center to the edge of the detector, is clearly visible. Soft proton flares observed by XMM-Newton also show a vignetted pattern, an effect that helped to identify their focused origin, with a decrease from the inner to the outer region of $\sim 50\%$,[27] similarly to our findings.

6. CONCLUSIONS

A prototype proton response matrix for the XMM-Newton telescope, selecting the medium optical filter and the MOS camera as focal plane assembly configuration, is described in its design and characterization, with the final goal of validating the simulation of the soft proton induced X-ray background against in-flight data and provide the community with an unprecedented tool for studying the near-Earth low energy radiation environment. The Geant4 implementation of the MOS front-illumination structure and the optical filter placed in the line of sight is successfully verified against on-ground measurements of the X-ray detection efficiency and analytical computations based on stopping power tabulated values. The simulation and analysis pipeline is verified by computing soft proton spectra, counts map and vignetting distribution using the ray-tracing elastic Remizovich

solution as physics scattering model at the X-ray optics. The simulation campaign for the production of the first release of the proton response matrix is now starting using both the ray-tracing and Geant4 simulation codes for the proton scattering at the mirror module.
Current estimates[28] for the Athena X-ray observatory show that the soft proton induced X-ray background is expected to be a few times to orders of magnitude higher than the required level, depending on the mission orbit. As a consequence, a magnetic diverter for charged particles[29] is currently foreseen on board the Athena spacecraft, on top of each of the instrument systems. Once the XMM-Newton proton response matrix is successfully compared against observations, we plan to apply the same simulation and analysis pipeline to build a proton response matrix for the Athena telescope to assess the shielding efficiency and driving potential optimizations of the diverter design.

ACKNOWLEDGMENTS

The research leading to these results has received funding from the European Union's Horizon 2020 Programme under the AHEAD2020 project (grant agreement n. 871158).

REFERENCES

[1] O'Dell, S. L. et al., "Radiation environment of the Chandra X-Ray Observatory," *Proc. of SPIE* **4140**, 99–110 (2000).
[2] Fioretti, V. et al., "Monte Carlo simulations of soft proton flares: testing the physics with XMM-Newton," *Proc. of SPIE* **9905**, 99056W (2016).
[3] Marelli, M. et al., "A systematic analysis of the XMM-Newton background: I. Dataset and extraction procedures," *Experimental Astronomy* **44**(3), 297–308 (2017).
[4] Lotti, S. et al., "Soft proton flux on ATHENA focal plane and its impact on the magnetic diverter design," *Experimental Astronomy* **45**(3), 411–428 (2018).
[5] Salvetti, D. et al., "A systematic analysis of the XMM-Newton background: II. Properties of the in-Field-Of-View excess component," *Experimental Astronomy* **44**(3), 309–320 (2017).
[6] Diebold, S. et al., "Updates on experimental grazing angle soft proton scattering," *Proc. of SPIE* **10397**, 103970W (2017).
[7] Macculi, C. et al., "AREMBES Final Report," *Project report, ATHENA Radiation Environment Models and X-ray Background Effects Simulators, ESA Contract No. 4000116655/16/NL/BW* (2021).
[8] Mineo, T. et al., "An XMM-Newton proton response matrix," *Experimental Astronomy* **44**(3), 287–296 (2017).
[9] Arnaud, K. A., "XSPEC: The First Ten Years," in [*ADASS V*], Jacoby, G. H. and Barnes, J., eds., *ASPC Series* **101**, 17 (1996).
[10] Kaastra, J. S., Mewe, R., and Nieuwenhuijzen, H., "SPEX: a new code for spectral analysis of X & UV spectra.," *UV and X-ray Spectroscopy of Astrophysical and Laboratory Plasmas* , 411–414 (1996).
[11] Agostinelli, S. et al., "Geant4–a simulation toolkit," *NIM A* **506**, 250 – 303 (2003).
[12] Allison, J. et al., "Geant4 developments and applications," *IEEE Trans. Nucl. Sci.* **53**(1), 270 –278 (2006).
[13] Jansen, F. et al., "Xmm-newton observatory. i. the spacecraft and operations," *A&A* **365**, L1–L6 (2001).
[14] Fioretti, V. et al., "Geant4 simulations of soft proton scattering in X-ray optics. A tentative validation using laboratory measurements," *Experimental Astronomy* **44**(3), 413–435 (2017).
[15] Diebold, S. et al., "Soft proton scattering efficiency measurements on x-ray mirror shells," *Experimental Astronomy* **39**, 343–365 (2015).
[16] Fioretti, V. et al., "EXACRAD WP 8.1 – Model validation results and recommendations for future work," *ESA EXACRAD Technical Note* (2021).
[17] Henke, B. L., Gullikson, E. M., and Davis, J. C., "X-Ray Interactions: Photoabsorption, Scattering, Transmission, and Reflection at E = 50-30,000 eV, Z = 1-92," *Atomic Data and Nuclear Data Tables* **54**(2), 181–342 (1993).
[18] Owens, A. et al., "Measuring reflected x-ray absorption fine structure in gold-coated x-ray mirrors," *Proc. of SPIE* **2279**, 325–331 (1994).

[19] Remizovich, V. S., Ryazanov, M. I., and Tilinin, I. S., "Energy and angular distributions of particles reflected in glancing incidence of a beam of ions on the surface of a material," *Sov. J. Exp. Th. Phys.* **52**, 225 (1980).
[20] Amato, R. et al., "Soft proton scattering at grazing incidence from X-ray mirrors: analysis of experimental data in the framework of the non-elastic approximation," *Experimental Astronomy* **49**(3), 115–140 (2020).
[21] Turner, M. J. L. et al., "The European Photon Imaging Camera on XMM-Newton: The MOS cameras," *A&A* **365**, L27–L35 (2001).
[22] Strüder, L. et al., "The european photon imaging camera on xmm-newton: The pn-ccd camera," *A&A* **365**, L18–L26 (2001).
[23] Holland, A. D. et al., "MOS CCDs for the EPIC on XMM," *Proc. of SPIE* **2808**, 414–420 (1996).
[24] Hiraga, J. et al., "Direct measurement of sub-pixel structure of the EPIC MOS CCD on-board the XMM//NEWTON satellite," *Nuclear Instruments and Methods in Physics Research A* **465**(2-3), 384–393 (2001).
[25] Fraser, G. W. et al., "Potential solar axion signatures in X-ray observations with the XMM-Newton observatory," *MNRAS* **445**(2), 2146–2168 (2014).
[26] De Luca, A. and Molendi, S., "The 2-8 keV cosmic X-ray background spectrum as observed with XMM-Newton," *A&A* **419**, 837–848 (2004).
[27] Strueder, L. et al., "X-ray pn-CCDs on the XMM Newton Observatory," *Proc. of SPIE* **4012**, 342–352 (2000).
[28] Fioretti, V. et al., "Magnetic Shielding of Soft Protons in Future X-Ray Telescopes: The Case of the ATHENA Wide Field Imager," *ApJ* **867**(1), 9 (2018).
[29] Ferreira, I. et al., "Design of the charged particle diverter for the ATHENA mission," *Proc. of SPIE* **10699**, 106994A (2018).